Fully coupled time domain solution for hydroelastic analysis of a floating body

Article *in* Ocean Engineering · February 2018

DOI: 10.1016/j.oceaneng.2018.01.061

3 authors, including:

Sumit Kumar Pal
Osaka University
9 PUBLICATIONS **7** CITATIONS
SEE PROFILE

Ranadev Datta
Indian Institute of Technology Kharagpur
22 PUBLICATIONS **93** CITATIONS
SEE PROFILE

Ocean Engineering 153 (2018) 173–184

Contents lists available at ScienceDirect

Ocean Engineering

journal homepage: www.elsevier.com/locate/oceaneng

Fully coupled time domain solution for hydroelastic analysis of a floating body

S.K. Pal [a,*], R. Datta [a], M.R. Sunny [a,b]

[a] Dept. of Ocean Engineering & Naval Architecture, IIT-Kharagpur, Kharagpur, West Bengal, 721302, India
[b] Dept. of Aerospace Engineering, IIT-Kharagpur, Kharagpur, West Bengal, 721302, India

ARTICLE INFO

Keywords:
Hydroelasticity
Time domain panel method
Transient free surface Green's function
Finite element method
Newmark - β method

ABSTRACT

A numerical method is developed to study the ship hydroelasticity problem in time domain. Boundary – Element Method (BEM) with three-dimensional transient free-surface Green function and Neumann – Kelvin approximation is used for the solution of the hydrodynamic part. The structural domain is modeled by finite element method (FEM) using 1D beam element in time domain. The coupling between BEM and FEM is made through body boundary condition in the hydrodynamic solution. Furthermore, direct integration scheme, i.e. Newmark –β method is used for obtaining the structural velocity and deformation. The efficiency and robustness of the proposed method are validated with available published results. Three different barge type structures and a large container ship are taken for the analysis. A good correspondence is observed between the proposed and reported numerical and experimental results. Also, it is observed that structural flexibility plays an important role while calculating structural deflection, shear force, bending moment etc. The developed numerical method seems to be robust, efficient and a very useful tool in predicting the hydrodynamic loads, structural deflections, shears force, bending moment etc. for flexible structure.

1. Introduction

Prediction of wave-induced loads and motions are two major aspects while designing a ship or offshore structures. Recently, commercial ships have been becoming larger and faster due to the increase in global trade. Large floating structures and ships are relatively more flexible and their natural frequencies can fall into the range of the encounter frequencies of commonly occurring sea spectrum. Similarly, with the increase in ship speed, the encounter frequency increases and more often may come closer to the natural frequencies of the ship hull vibration. In such situations, the hydrodynamic loads on the structure and corresponding structural responses become large and leads to severe structural damage. Therefore it is important to develop a proper fluid-structure interaction model to predict the wave-induced loads and structural responses in such extreme situations.

A classical hydroelastic tool to analyze the interaction between the fluid and large floating structures was developed by Bishop and Price (1979). Since then, many researchers have contributed to the various aspects of this field. Different numerical techniques were also proposed by many researchers for the solution of such practical engineering problems.

Generally, a hydroelastic model can broadly divide into three major components: (i) hydrodynamic model to estimate the hydrodynamic load on the structure, (ii) structural model to predict the structural deflections and (iii) coupling of the hydrodynamic and structural model.

In case of simplified structures such as two dimensional rectangular and circular plates, many rigorous and complete analytic solutions are available. Some of the recent works in these lines are as follows; Sahoo et al. (2001) analyzed scattering of surface waves by a semi-infinite floating elastic plate. An extensive study on the hydroelasticity of a very large structure was given by Andrianov (2005). Squire (2008) developed a contemporary hydroelastic theory to describe how sea ice responds to an ocean wave field and those that relate to a very large floating structure (VLFS) experiencing comparable forcing. Karmakar et al. (2009) studied wave interaction with multiple articulated floating elastic plates etc. Meylan and Sturova (2009) proposed three methods to determine the motion of a two-dimensional finite elastic plate floating on the water surface. Recently, Wang et al. (2016) investigated the hydroelastic response of a horizontal elastic plate impacting with the water both theoretically and numerically.

In order to develop a robust and efficient method for hydroelastic analysis for the complicated structures like a ship, it is essential to

* Corresponding author.
E-mail address: sumitkpal@iitkgp.ac.in (S.K. Pal).

https://doi.org/10.1016/j.oceaneng.2018.01.061
Received 21 July 2017; Received in revised form 24 November 2017; Accepted 13 January 2018

develop a coupled hydrodynamic-structural solver either in frequency or time domain. For the frequency domain solutions, some examples are as follows: A detailed investigations of ship hydroelasticity of a bulk carrier is elaborated in Hirdaris et al. (2003). Timoshenko beam idealization with shear center influence and warping effects were included, and finite difference formulations, as well as 3D FEM model, were employed. Both models were combined with potential flow theory in the frequency domain. Iijima et al. (2008) proposed a consistent structural analysis procedure to estimate the global and local load effects considering symmetric and anti-symmetric hydroelastic vibrations to study the structural response of a ship in severe seas. Senjanovic et al. (2008a, 2008b, 2009) extensively investigated the problem of hydroelasticity of ships with many details. The hydrodynamic problem was solved in frequency domain either using strip theory or 3D Boundary element method (BEM) whereas the structural dynamic problem solved using 1D/3D Finite element method (FEM). Meylan and Tomic (2012) introduced a method that explained the behaviour of an elastic or rigid structure by its resonance frequencies. This study provided some fundamental information that could be of use in giving a simplified description for the response of complicated structures.

The time domain solvers are capable of addressing certain nonlinear effects such as Froude-Krylov nonlinearity, nonlinear hydrostatics, and structural nonlinearity etc. in a relatively straightforward way and thus advantageous over frequency domain solvers. Also for a forward moving vessel, time domain solutions are found to be less complicated in comparison to frequency domain solutions. Therefore a significant effort is made to solve the hydroelasticity problem in the time domain as well.

While dealing with the ship hydroelasticity problem in the time domain, one of the most popular methods is to solve through Impulse Response Function (IRF), i.e. extending Cummin's (1962) formulation for flexible body together with FEM or modal superposition method. Wu and Moan (1996) developed a nonlinear hydroelastic method where the linear part was calculated using linear strip theory and nonlinear modification was made from linear impulse response function. Taghipour et al. (2009) developed a state-space model using IRF to deal with the time-domain hydroelastic analysis of a marine structure. Rajendran and Guedes Soares (2016) investigated the response of a very large container ship in rough sea, where the radiation forces were obtained using IRF and the structural problem was solved using finite element method. Generally, the idea behind such efforts is to use time domain method based on IRF to include the several nonlinearities in a simplified way or to combine CFD solver with the hydroelasticity solution. For example, Rajendran and Guedes Soares (2016) included the nonlinear radiation and diffraction force in a simplified manner. Seng et al. (2014) included the local effect through Volume of fluid (VOF)-based free surface flow solver in hydroelasticity solution, where hydroelasticity solver is based on IRF based time domain technique.

The numerical technique based on IRF requires frequency domain solution. However, without such information, the problem of hydroelasticity can be handled in the time domain using direct coupling between hydrodynamic and structural solution. Relatively less reported, but few researchers have worked on such direct coupling as well. In these cases, the hydrodynamic solver is developed using time domain boundary element method and coupled with a finite element or modal superposition technique based on the structural dynamic solver. A very systematic study has been done by Kim et al. (2009, 2013), they coupled Rankine panel method and FEM to study the hydroelasticity of ships like structure in waves. Kara (2015) used transient free surface Green's function based time domain panel method to calculate the hydrodynamic loads. However, the structural problem was solved using modal superposition technique assuming the ship to be a free-free Euler-Bernoulli beam.

Direct coupling between BEM and FEM solver offer certain advantages; for example, (i) It implicitly takes all the wet modes of structural vibration. (ii) Extending this theory to include forward speed is relatively easier. (iii) Extension of the linear model into a nonlinear model for both hydrodynamic and structural part is possible in principle, etc.

In view of that, in the present study, the problem of ship hydroelasticity has been solved by a direct coupling of a BEM and a FEM based solver. For the hydrodynamic solution, a 3D time domain panel method using transient free surface Green's function is used by following the approach of Kara (2015). For the structural part, 1D finite element beam model is used for analysis of the structural deformation, shear force, bending moment etc. The coupling between hydrodynamic and structural dynamic solvers is made through kinematic body boundary condition. The dynamic responses of the structure are then found out at each time step by Newmark -β method. The validation of the time domain panel method code used in this paper has been extensively done and reported in many literatures (Datta et al., 2011, 2013; Sengupta et al., 2016) in case of linear and nonlinear seakeeping problem. In this paper, an extension to that code for hydroelasticity analysis is elaborated. A very brief discussion of the present method is reported in Sengupta et al. (2017). An elaborate discussion on the methodology and validation is given in this paper. For validating the hydroelastic solution, three different types of barges and a large container ship without forward speed are taken for the analysis. The vertical bending moment (VBM), shear force (SF) are calculated and computed results are compared with existing published numerical and experimental results and found satisfactory agreement between them.

2. Mathematical formulation and numerical implementation

2.1. Numerical formulation of the structural problem

In this paper, the ship hull has been modeled as an Euler-Bernoulli beam floating in the water. Considering the basic assumptions of an Euler-Bernoulli beam, the response of the ship hull due to the external force $f(x,t)$ can be described by the following governing differential equation:

$$m(x)\frac{\partial^2 w}{\partial t^2}+\frac{\partial^2}{\partial x^2}\left(EI(x)\frac{\partial^2 w}{\partial x^2}\right)=f(x,t) \tag{1}$$

In equation (1), $m(x)$ is the mass per unit length of the structure, $EI(x)$ represents flexural rigidity along the length of the structure, w is the elastic deflection of the floating body. The calculation of mass distribution depends on the structural arrangements inside the hull and the cargo distributions. However, the distribution of flexural rigidity is usually calculated from the actual geometric shape of the different cross-sections along the hull.

The weak form representation of equation (1) is obtained by multiplying it with weighted function v and integrating it over the domain $\Omega_s(0,L)$.

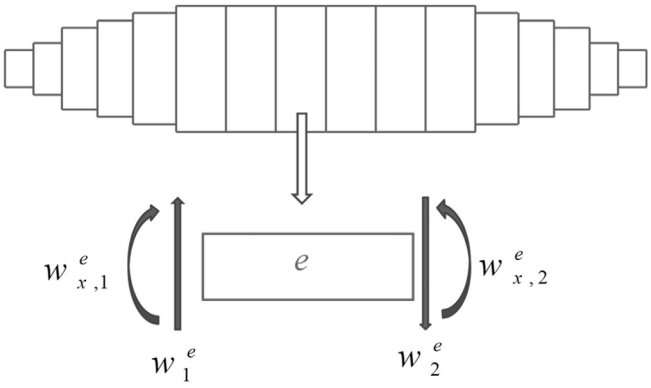

Fig. 1. Non-uniform beam idealization of the ship and degrees of freedom of an element.

$$\int_0^L m(x)\frac{\partial^2 w}{\partial t^2}v\,dx + \int_0^L \frac{\partial^2}{\partial x^2}\left(EI(x)\frac{\partial^2 w}{\partial x^2}\right)v\,dx - \int_0^L fv\,dx = 0 \tag{2}$$

Assuming the uniform distribution of the weighted function, v and dependent variable, w, equation (2) can be further modified as,

$$\int_0^L m(x)\frac{\partial^2 w}{\partial t^2}v\,dx + \int_0^L EI(x)\frac{\partial^2 v}{\partial x^2}\frac{\partial^2 w}{\partial x^2}dx - \int_0^L fv\,dx = 0 \tag{3}$$

The hull girder is discretized into a set of N_e elements whilst, each element consists of two nodes. Since in the present formulation, only vertical displacement and rotational displacement about transverse axis is considered, two degrees of freedom is taken at each node and denoted by $w_{\ i}$ and $w_{x,\ i}$ where $w_{x,\ i} \equiv \partial w/\partial x|_{i^{th}node}$ (see Fig. 1). Thus at any point, the displacement w and the weighted function v can be written as:

$$w = \sum_{i=1}^{4} d_i^e N_i^e \tag{4a}$$

$$v = \sum_{j=1}^{4} g_j^e N_j^e \tag{4b}$$

In above equations $N^e : \{N_1^e, N_2^e, N_3^e, N_4^e\}$ represents Hermite shape functions of the individual degrees of freedom and $d^e : \{w_1^e, w_{x,1}^e, w_2^e, w_{x,2}^e\}$ represents degrees of freedom at element e.

In equation (4b), v is arbitrary and satisfies only the homogeneous version of the essential boundary condition. Therefore, g_j has to be arbitrary and for each g_j there will be an algebraic equation.

Substituting the approximations for w and v into equation (3) yields,

$$\sum_{e=1}^{N_e}\left[\sum_{j=1}^{4} g_j^e\left\{\sum_{i=1}^{4}\left(\int_0^{l_e} m(x)N_i^e N_j^e \ddot{d}_i^e dx + \int_0^{l_e} EI(x)\frac{\partial^2 N_i^e}{\partial x^2}\frac{\partial^2 N_j^e}{\partial x^2}d_i^e dx - \int_0^{l_e} fN_j^e dx\right)\right\}\right] = 0 \tag{5}$$

After simplification, the elemental equation turns out as,

$$[M^e]_{4\times4}\left\{\ddot{d}_i^e\right\}_{4\times1} + [K^e]_{4\times4}\left\{d_i^e\right\}_{4\times1} = \left\{F_i^e\right\}_{4\times1} \tag{6}$$

In equation (6) the expressions for mass matrix, stiffness matrix and force vector of an element e, can be given as,

$$M_{ij}^e = \int_0^{l_e} m(x)N_i^e N_j^e dx \tag{7}$$

$$K_{ij}^e = \int_0^{l_e}\left(EI(x)\frac{\partial^2 N_i^e}{\partial x^2}\frac{\partial^2 N_j^e}{\partial x^2}\right)dx \tag{8}$$

$$F_i^e = \int_0^{l_e} f\,N_j^e dx \tag{9}$$

Equation (6) is a system of four linear simultaneous ordinary differential equations. Combining these elemental equations with consideration to the nodal connectivity of different elements, the global finite element equation (10) can be obtained. Since an accurate simulation of the system damping is difficult, in the current study an approximate method using Rayleigh damping model (Liu and Gorman, 1995) is used and expressed as $[C] = \alpha_d[K] + \beta_d[M]$, where α_d and β_d are the proportional coefficients for the stiffness and mass, respectively. The values of α_d and β_d are calculated as 0.001 and 0.0001 using the procedure mentioned in Liu et al. (2016). Adding this Rayleigh damping term, the final global finite element equation can be obtained as,

$$[M]\{\ddot{d}\} + [C]\{\dot{d}\} + [K]\{d\} = \{F\} \tag{10}$$

Herein, $[M]$ and $[K]$ are the global mass and stiffness matrices, $\{F\}$ is the global force vector.

2.2. Hydrodynamic analysis

In equation (10), external force $\{F\}$ is the wave induced loads and moments which is obtained by solving the hydrodynamic problem. The boundary value problem for the hydrodynamic solution can be stated as follows:

Assuming the fluid is homogeneous, inviscid and incompressible and flow is ir-rotational. Then based on the potential flow assumptions, the total velocity potential $\phi_T(\vec{X}, t)$ can be defined as:

$$\phi_T(\vec{X}, t) = \phi_I(\vec{X}, t) + \phi(\vec{X}, t) \tag{11}$$

In equation (11), $\phi_I(\vec{X}, t)$ is the incident wave potential, $\phi(\vec{X}, t)$ represents the disturbed potential which is combination of radiation and diffraction potential. The linearized initial boundary value problem for $\phi(\vec{X}, t)$ is specified by the following governing equations, boundary conditions, far field conditions and one initial condition as follows:

$\phi(\vec{X}, t)$ satisfies the Laplace equation in the fluid domain Ω_f, i.e.

$$\nabla^2\phi(\vec{X}; t) = 0; \quad \vec{X} \in \Omega_f \tag{12}$$

The linearized free surface boundary condition can be given by:

$$\frac{\partial^2\phi}{\partial t^2} + g\frac{\partial\phi}{\partial z} = 0 \quad \text{on } z = 0 \tag{13}$$

where g denotes the acceleration due to gravity. The kinematic body boundary condition for hydroelasticity solution is different from rigid body case. In case of rigid body, the kinematic body boundary condition can be written as:

$$\frac{\partial\phi}{\partial n} = \overline{V}(t).\overline{n} - \frac{\partial\phi_I}{\partial n} \quad \text{on } S_0 \tag{14a}$$

In (14a), $\overline{V}(t)$ is the velocity of the rigid body at its center of gravity at the time t and S_0 is the mean wetted surface. $\overline{n}$ denotes the unit normal to the body. However, in case of deformable body, the velocity is varying along the horizontal, transverse and vertical axis and therefore the velocity of the body becomes the function of both $\vec{X}$ and t. Therefore, the body boundary condition for the deformable body can be expressed as

$$\frac{\partial\phi}{\partial n} = V(\vec{X}; t).\overline{n} - \frac{\partial\phi_I}{\partial n} \quad \text{on } S_0 \tag{14b}$$

Finally, the far field and initial condition can be written as:

$$\phi, \phi_t \to 0 \quad \text{as } R_H \to \infty, \quad \text{on } z = 0 \tag{15}$$

$$\phi, \ \phi_t \to 0 \quad \text{as } t \to 0 \tag{16}$$

In the above equations, $R_H = \sqrt{(x^2 + y^2)}$.

Although the body boundary condition is different from the rigid one, the integral equation does not change because of that. Using the time dependent (transient) Green's function, $\phi(\overline{p}, t)$ can be expressed in the form of an integral equation:

$$\phi(\overline{p},t) = -\frac{1}{4\pi}\left\{ \iint_{S_0} \sigma(\overline{q},t) G^o(\overline{p},\overline{q}) dS + \int_0^t d\tau \left[\iint_{S_0} \sigma(\overline{q},t) G_t^f(\overline{p},\overline{q};t-\tau) dS \right] \right\} \tag{17a}$$

Expression (17a) represents the total disturbance potential ϕ at any point p at any instant of time t in terms of distribution of sources over the body surface. In (17a), $\sigma(\overline{q},t)$ is the associated source strength at time t. Differentiating (17a) with respect to the normal vector and applying the boundary conditions at p in S_0 gives the following integral equation:

$$\frac{\partial\phi(\overline{p};t)}{\partial n_p} = -\frac{1}{4\pi}\left\{ \iint_{S_0} \sigma(\overline{q},t) \frac{\partial G^0(\overline{p},\overline{q})}{\partial n_p} dS + \int_0^t d\tau \left[\iint_{S_0} \sigma(\overline{q},t) \frac{\partial G_t^f(\overline{p},\overline{q};t-\tau)}{\partial n_p} dS \right] \right\} \tag{17b}$$

where,

$$G^0 = \frac{1}{r} - \frac{1}{r'} \tag{17c}$$

$$G^f = 2\int_0^\infty \left[1 - \cos(\sqrt{gk}(t-\tau)\right] e^{k(z+\zeta)} J_o(kR) dk \tag{17d}$$

$$r = |p-q| = \sqrt{(x-\xi)^2 + (y-\eta)^2 + (z-\zeta)^2} \tag{17e}$$

$$r' = |p-q'| = \sqrt{(x-\xi)^2 + (y-\eta)^2 + (z+\zeta)^2} \tag{17f}$$

$$R = \sqrt{(x-\xi)^2 + (y-\eta)^2} \tag{17g}$$

$$J_0 = \text{Bessel function of the first kind of order zero.} \tag{17h}$$

In the above, G^0 and G^f represent the Rankine part and the free-surface memory part of the Green's function respectively, $p(x,y,z)$ and $q(\xi,\eta,\zeta)$ are the field and the source points, $q' = (\xi,\eta,-\zeta)$ is the image of q above the mean free surface $z = 0$, k is the wave number, and G_t^f is the derivation of the G^f with respect to τ. The detail on the formation of the integral relation and the expression for G^o and G^f is available in many sources, e.g., Lin and Yue (1990). Equation (17b) is used to solve for the unknown source strengths $\sigma(\overline{q},t)$. Once source strengths $\sigma(\overline{q},t)$ are known, equation (17a) is then applied to determine the unknowns $\phi(\overline{X},t)$ over the body surface. Once $\phi(\overline{X},t)$ over body surface is determined, pressure on the body can be found from the Bernoulli equation and the hydrodynamic force and moment can be determined by integrating pressure over the body surface.

Let $P(\overline{X},t)$ be the total dynamic pressure distribution including the hydrodynamic pressure due to disturbed potential $\phi(\overline{X},t)$ and pressure due to incident wave potential $\phi_I(\overline{X},t)$ at any arbitrary point on the body. Then, the total dynamic pressure on that point can be obtained from the equation:

$$P(\overline{X},t) = -\rho_0\left\{ \frac{\partial\phi(\overline{X},t)}{\partial t} + \frac{\partial\phi_I(\overline{X},t)}{\partial t} + \frac{1}{2}[(\nabla\phi) + (\nabla\phi_I)]^2 \right\} \tag{18}$$

In equation (18), ρ_0 is the density of the fluid. equation (18) is the general form of the pressure equation, for the zero speed problem, the quadratic contribution can be ignored. However, for the linearized problem with forward speed, in present earth fixed co-ordinate system, the quadratic contributions are included in the pressure equation for accounting the forward speed. The detailed discussion on the same can be found in Lin and Yue (1990).

Therefore the dynamic force $F_{S_X}(t)$ due to pressure $P(\overline{X},t)$ at any arbitrary section S_X at any instant of time t can be obtained as:

$$F_{S_X}(t) = \iint_{S_X(t)} P(\overline{X},t).\overline{n}.dS_X \tag{19}$$

The dynamic force obtained from (19) along with hydrostatic force can be taken as an external force for the solution of the structural problem. Once the structural problem solved in the time domain, the body boundary condition (14b) will be updated accordingly to solve the boundary value problem. The details of this coupling will be discussed in the following sections.

2.3. Numerical solution of the hydrodynamic problem

A lower order panel method is used to solve the hydrodynamic problem. In lower order panel method, the velocity potential is assumed to be constant over a panel. Therefore it simplifies the nature of continuous variation of the velocity potential over the wetted surface. In order to capture these phenomena more appropriately, a higher order panel method proposed by Kim et al. (2009, 2013) would be the better choice. However, one can always overcome this limitation by making panel size sufficiently small.

The discretized form of the body boundary condition (14b) for the arbitrary panel i can be given as:

$$\left(\frac{\partial\phi}{\partial n}\right)_i = \overline{V}_i.\overline{n}_i - \left(\frac{\partial\phi}{\partial n}\right)_i \tag{20}$$

In the above equation, $\overline{V}_i$ represents the velocity at the centroid of the i^{th} panel, $\overline{n}_i$ is the generalized normal vector to the i^{th} panel. Since the present formulation based on constant-element boundary element implementation along with a trapezoidal rule for the convolution integral, following steps have been followed:

(i) Discretize S_0 by N planar quadrilateral and triangular panels.
(ii) Assume σ to be constant over the panels and over the line segments with values same as at the centroid of the panels (note that the source strength over the line segments becomes same as the source strength of the adjacent panel).
(iii) Assume time-step size Δt to be constant in carrying out the time integration and use a forward-step Euler method.
(iv) Use trapezoidal rule for the convolution integration.

This reduces the integrals to a system of linear equations in terms of the discrete source strengths and potentials. For example, (17a) reduces to:

$$\phi_j = -\frac{1}{4\pi}\sum_{j=1}^{N}\sigma_j \iint_{\Delta S_j} G^0\left(p_i(t),q_j(\tau)\right)dS - \Delta t\sum_{m=0}^{M-1}\varepsilon_m\left[\sigma_j \iint_{\Delta S_j} G^f\left(p_i(t),q_j(\tau)\right)dS\right]; i = 1,\ldots,N \tag{21a}$$

$$\sum_{j=1}^{N}\sigma_j^M \iint_{\Delta S_j}\frac{\partial}{\partial n_i}G^0\left(p_i(t),q_j(\tau)\right)dS = -4\pi[V(p_i(t)) - \nabla\phi_I(p_i(t))].n_i - \Delta t\sum_{m=0}^{M-1}\varepsilon_m\left[\sum_{j=1}^{N}\sigma_j \iint_{\Delta S_j}\frac{\partial}{\partial n_i}G^f\left(p_i(t),q_j(\tau)\right)dS\right]; \quad i = 1,\ldots,N \tag{21b}$$

In similar fashion, $\nabla\phi_j^M$ can be obtained from the following equation as:

$$\nabla\phi_j^M = -\frac{1}{4\pi}\sum_{j=1}^{N}\sigma_j^M \iint_{\Delta S_j}\nabla G^0\left(p_i(t),q_j(\tau)\right)dS - \Delta t\sum_{m=0}^{M-1}\varepsilon_m\left[\sigma_j^m \iint_{\Delta S_j}\nabla G^f\left(p_i(t),q_j(\tau)\right)dS\right];\ \ i=1,\ldots,N \tag{21c}$$

Here, M and m are indices for the current time t and retarded time τ: $t = M\Delta t$, $\tau = m\Delta t$, i and j are the indices for the field point p and source point q respectively, $\varepsilon = 0.5$ for $m = 0$ and 1 for $m > 1$. For integration of the memory part of the Green function over the panels, four point Gauss quadrature rules are used, while the Rankine part is integrated using a combination of analytical formula and quadrature rules of variable order in order to achieve consistent level of accuracy over the entire computational domain. For the self influencing panel, the analytical formulation proposed by Newman (1986) is adopted. The detailed discussion on the numerical integration scheme is available in many literatures (for example: Sen, 2002; Datta and Sen, 2007) and not repeated here.

Once the distribution of unknown $\phi(\overline{X},t)$ over the mean wetted surface is known, dynamic pressure at the centroid of the panel can be found out through equation (18). Finally, the dynamic force acted at any arbitrary panel i can be obtained as:

$$\overline{F}_i^M(t) = P_i^M.\overline{n}_i.ds_i \tag{22}$$

In the above expression, $\overline{F}_i^M(t)$ is the dynamic force at panel i at M^{th} time step. P_i^M is the pressure at the Centroid of the panel i at M^{th} time step. ds_i is the area of i^{th} panel at $t = 0$. In reality, the panel area and the unit normal should be the function of time. However, by taking sufficiently small panels, one can assume that the variation in the panel area is ignorable. Such simplification would not affect the final solution as $\delta(ds_i) \approx O(\varepsilon^2)$. On the other hand, the change in normal velocity is taken care in appropriate manner. Therefore in the present paper, the panel normal for the deformed shape is stored at each time step to calculate the variation of the normal with time. However, under the assumptions of the linearity, panels co-ordinates are not updated.

2.4. Modelling of restoring force

Modelling of restoring force is not straightforward in comparison to the rigid body case. A detailed discussion on modelling of restoring force and its effect on the hydroelastic solution is deeply studied by Senjanović et al. (2008b). In their derivations, modeshapes are taken explicitly. The present formulation is based on finite element method where modeshapes are implicitly defined. Therefore in this paper, an alternative solution proposed by Kim et al. (2009) is adopted. Here, the restoring force at the i^{th} panel is written as:

$$F_i^{restoring}(t) = -\rho_0 g\overline{Z}_i\delta\overline{n}_i.ds_i - \rho_0 g\delta\overline{Z}_i\overline{n}_i.ds_i \tag{23}$$

where, $\overline{Z}_i$ are water head and δ denotes the leading order variation.

2.5. Coupling between BEM and FEM in time domain

The structural and hydrodynamic problems are solved through the global finite element equation (10) and the boundary element equations (17)–(19), respectively. The global finite element equation (10) has been solved using Newmark's time integration method (Newmark, 1959). According to the Newmark's method, nodal displacement vector $\{d\}$ at any time instant t can be related to $\{d\}$ at the previous time instant by the following equation:

$$\left(\frac{[M]}{\alpha\Delta t^2}+\frac{\delta}{\alpha\Delta t}[C]+[K]\right)\{d\}_t = \{F\}_t + [M]\left[\frac{1}{\alpha\Delta t^2}\{d\}_{t-\Delta t}+\frac{1}{\alpha\Delta t}\{\dot{d}\}_{t-\Delta t}+\left(\frac{1}{2\alpha}-1\right)\{\ddot{d}\}_{t-\Delta t}\right] + [C]\left[\frac{\delta}{\alpha\Delta t}\{d\}_{t-\Delta t}+\left(\frac{\delta}{\alpha}-1\right)\{\dot{d}\}_{t-\Delta t}+\frac{\Delta t}{2}\left(\frac{\delta}{\alpha}-2\right)\{\ddot{d}\}_{t-\Delta t}\right] \tag{24}$$

After calculating $\{d\}$, the velocities and acceleration vectors can be calculated using the following equations.

$$\{\ddot{d}\}_t = \frac{1}{\alpha\Delta t^2}(\{d\}_t - \{d\}_{t-\Delta t}) - \frac{1}{\alpha\Delta t}\{\dot{d}\}_{t-\Delta t} - \left(\frac{1}{2\alpha}-1\right)\{\ddot{d}\}_{t-\Delta t} \tag{25}$$

$$\{\dot{d}\}_t = \{\dot{d}\}_{t-\Delta t} + \Delta t\left[(1-\delta)\{\ddot{d}\}_{t-\Delta t} + \delta\{\ddot{d}\}_t\right] \tag{26}$$

The parameters α and δ decide stability and accuracy of the method and describe the variation of acceleration over a time step. The values of α and δ are generally taken as $1/4$ and $1/2$ (Kim et al., 2013) and same values are taken in this work as well. Using the velocities obtained from equation (26), force can be calculated from equations (17)–(19). Using this force with the help of equations (24)–(26), the displacement, velocity, and acceleration vectors can be obtained for the next time step. In this way, the time marching is continued.

Solution of equation (10) gives unknown structural responses at each node of the finite element model. However, to solve equation (10), force per unit length f is required. The external force, f at different nodes is obtained by solving the hydrodynamic problem, i.e. boundary element equations (17)–(19). On the other hand, to get the hydrodynamic force, structural velocity and displacement at each node are required which can only be obtained by solving equation (10). Therefore, a suitable coupling scheme is required for exchanging the variables between the finite element and boundary element equations. An efficient algorithm is proposed in this paper for such coupling.

Normally, the hydrodynamic panel and finite element grids are different. Moreover, the hydrodynamic loads are computed at panel centroid, but structural velocity is calculated at sections. Therefore, it is important to shift the panel force to sectional force and sectional velocity

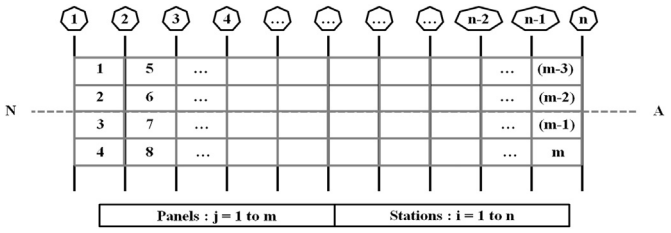

Fig. 2. Schematically representation of panel and station divisions.

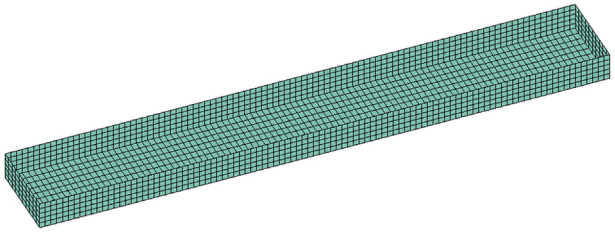

Fig. 3. Panel model of the Barge used for hydrodynamic analysis.

Table 1
The principal particulars of the Barge.

Item	Symbol	Value
Length over all (m)	*LOA*	120.0
Length between perpendiculars (m)	*LBP*	120.0
Breadth (m)	*B*	12.0
Draught (m)	*T*	6.0
Displacement (tonnes)	*M*	8856.0
Distributed mass (t/m)	*m*	73.8
LCG from mid-ship (m)		0.0
Radius of Gyration about x-axis (m)	k_{xx}	3.46
Radius of Gyration about y-axis (m)	k_{yy}	28.86
Radius of Gyration about z-axis (m)	k_{zz}	28.86

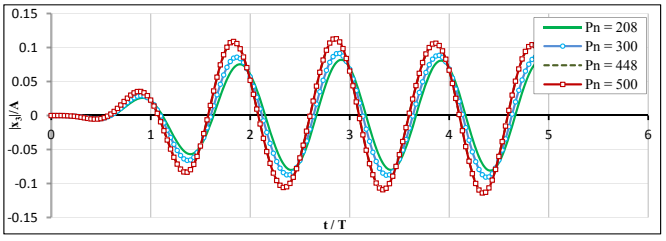

Fig. 4. Vertical displacement at mid-ship of the Barge at different discretization for $\omega\sqrt{L/g}$= **2.5**.

Table 2
Dry natural frequencies (Hz) of the first four flexible vertical modes of the Barge.

Mode No.	$N_n = 25$	$N_n = 50$	$N_n = 100$	$N_n = 150$	Analytical (Sengupta et al., 2016)
7	5.4419	5.4419	5.4419	5.4419	5.4417
8	15.001	15.001	15.001	15.001	14.9999
9	29.408	29.408	29.407	29.407	29.4095
10	48.616	48.612	48.612	48.612	48.6108

and displacement to panel velocity and displacement. Fig. 2 shows the schematic diagram of the positions of the panels and stations in a simplistic way. It can be seen from Fig. 2 that panels are arranged in such a way that none of the panels are intersected by the section lines. This simplification reduces the complexity of incorporating the hydrodynamic load into the structural analysis. Furthermore, it is considered that the pressure, velocity etc. are linearly varying between two consecutive panels along the horizontal axis. In view of that, the vertical force per unit run, f is calculated at the stations as follows:

$$f(1) = \sum_{j=1}^{m} \frac{P^M(j)A_p(j)n(j)}{2W_p(j)} \quad for \quad X(j)|_{Panel} < S_2 \tag{27a}$$

$$f(n) = \sum_{j=1}^{m} \frac{P^M(j)A_p(j)n(j)}{2W_p(j)} \quad for \quad X(j)|_{Panel} > S_{n-1} \tag{27b}$$

$$f(i) = \sum_{j=1}^{m} \frac{P^M(j)A_p(j)n(j)}{2W_p(j)} \quad for \quad \begin{cases} X(j)|_{Panel} < S_{i+1} \\ X(j)|_{Panel} > S_{i-1} \end{cases} \tag{27c}$$

where, i and j are the index notation for station and panel numbering. The calculated hydrodynamic pressure at j^{th} panel centroid for the M^{th} time step is denoted here by $P^M(j)$. A_p is denoted as panel area, and panel width is given by W_p . $X(j)|_{Panel}$ represents the longitudinal position of the j^{th} panel and S_i denotes longitudinal location of i^{th} section respectively. In Fig. 2, m represents the number of hydrodynamic panel within the respective range, and n is the total number of structural grids.

After getting the sectional force using (27. a-c), Newmark -β method is applied in order to compute velocities at different nodes of the elements. Similarly, the velocity at panel centroid V is calculated from the velocities at different nodes using equation (28a-d).

$$V(i)|_{Station} = \dot{d}(2k-1) \quad for \quad S_i = x_1(k)|_{Element} \tag{28a}$$

$$V(i)|_{Station} = \dot{d}(2k+1) \quad for \quad S_i = x_2(k)|_{Element} \tag{28b}$$

$$V(i)|_{Station} = Interpolation \begin{cases} x_1(k)|_{Element} \rightarrow \dot{d}(2k-1) \\ x_2(k)|_{Element} \rightarrow \dot{d}(2k+1) \end{cases} \tag{28c}$$

$$V(j)|_{Panel} = Interpolation \begin{cases} V(i)|_{Station} \rightarrow S_i \\ V(i+1)|_{Station} \rightarrow S_{i+1} \end{cases} \tag{28d}$$

where, k is the index notation for element numbering; $x_1(k)|_{Element}$ and $x_2(k)|_{Element}$ are the longitudinal position of the 1st and 2nd node of an element e. Once the velocity at each panel centroid is obtained, the body boundary condition (14b) is updated for the next time step and corresponding hydrodynamic pressure is estimated using BEM. Thus, the coupling between FEM and BEM is made.

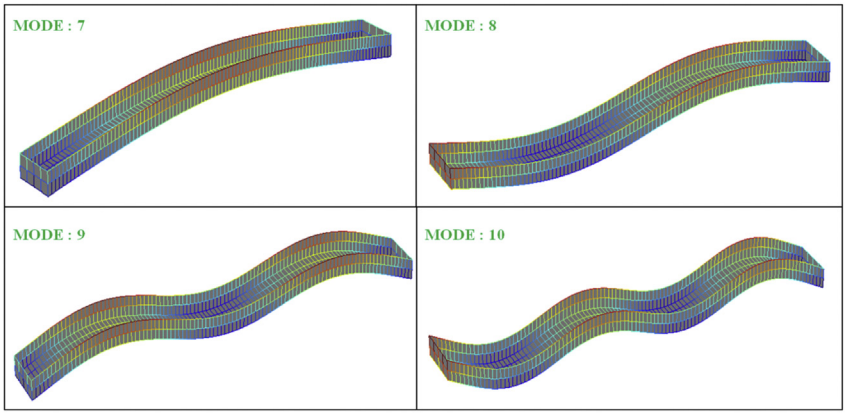

Fig. 5. First four flexible modes of vibration.

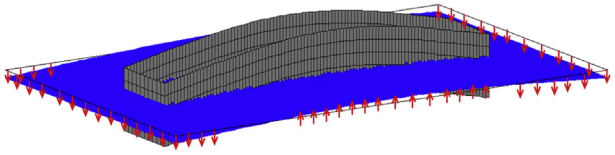

Fig. 6. $\delta\vec{n}$ on the body surface.

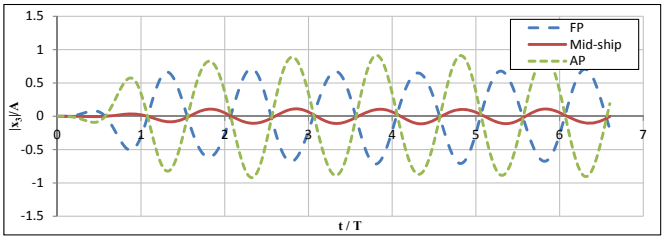

Fig. 7. Time histories of vertical displacement of the Barge, $F_n = 0.0$, $\beta = 180^\circ$, $\omega\sqrt{L/g} = 2.5$.

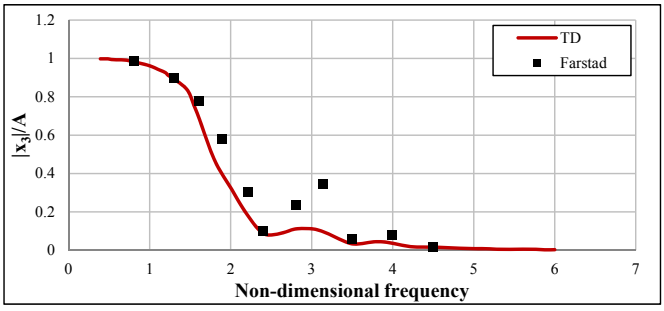

Fig. 8. Vertical displacement RAOs at mid-ship of the Barge.

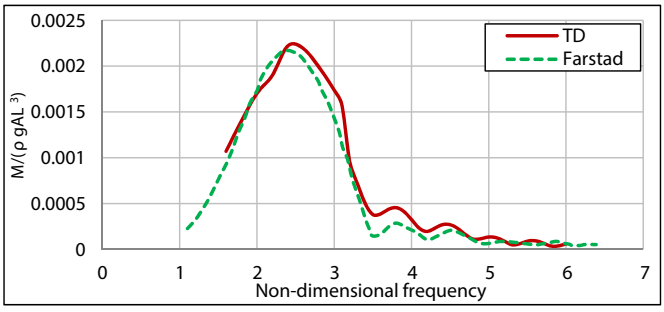

Fig. 9. Vertical Bending Moment transfer function at mid-ship of the Barge.

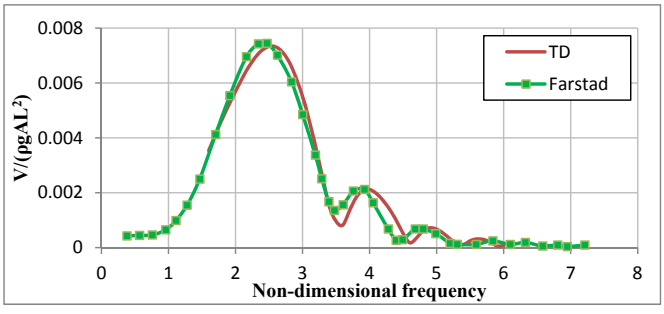

Fig. 10. Vertical Shear Force transfer function at (−) L/4 of mid-ship of the Barge.

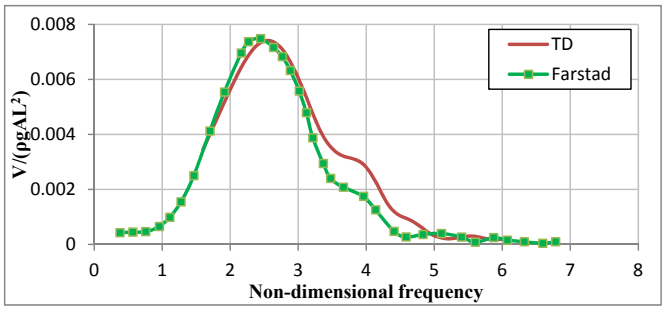

Fig. 11. Vertical Shear Force transfer function at (+) L/4 of mid-ship of the Barge.

3. Results and discussion

Three different types of barge and a containership are taken for the analysis. To demonstrate the efficiency and robustness of the proposed method, structural deflection, shear force, bending moment are calculated for the floating vessel without forward speed and compared with available experimental and numerical results.

The results obtained from the proposed method are referred as 'TD'. The frequency is non-dimensionalised by $\omega\sqrt{L/g}$, where, ω is the incident wave frequency, L is the length of the hull, g is the acceleration due to gravity. Time is non-dimensionalised by t/T, where T is the time period. Structural displacement at any section is non-dimensionalised by $|x_3|/A$, where $|x_3|$ is the magnitude of the displacement of that section and A denotes the wave amplitude. The shear force and bending moment are non-dimensionalised by $V/(\rho gAL^2)$ and $M/(\rho gAL^3)$, where, V and M represents the amplitude of shear force and bending moment.

3.1. Analysis for barge type structure

In the present paper, three different barge models are taken for the analysis named as Model I, Model II and Model III. The differences between these models lie in structural properties, geometric dimensions etc. The details of the same are discussed in the relevant sections.

3.1.1. Analysis of barge model I

The panel model for the barge is shown in Fig. 3 and the principal particulars of the barge are also presented in Table 1. In general, the hydrodynamic grid is different from the structural grid and therefore convergence study is essential for both the grids. For hydrodynamic analysis, the barge is discretized by a different set of panels to obtain the optimum panel size. The proper discretization of the hull is achieved through the convergence test. Fig. 4 shows the deflection at mid-ship of the barge for four different panel sizes at $\omega\sqrt{L/g} = 2.5$, which is essentially the case where wavelength to ship length ratio becomes approximately 1.0. From the figure, it is seen that convergence is achieved around 448 panels for the solution of the hydrodynamic part. Also from Fig. 4, it may be observed that all four plots are very stable with time. This indicates the efficiency and the robustness of the present time domain hydrodynamic code.

To obtain the optimum number of elements required for FEA, free vibration analysis is performed considering the ship as an equivalent Euler – Bernoulli beam, which is discretized with N_n number of nodes. The choice of the discretization is made through the convergence of the eigenfrequencies. In Table 2, the dry natural frequencies (Hz) of the first four flexible vertical modes of the barge are presented, and corresponding mode shapes are presented in Fig. 5. From Table 2 it can be confirmed that the natural frequencies in case of the barge are converged at $N_n = 100$. Also, the variation in body normal i.e. $\delta\vec{n}$ is plotted for a given time instance in Fig. 6. From the figure, it can be seen that variation of the normal vector is not ignorable and thus proper modelling of

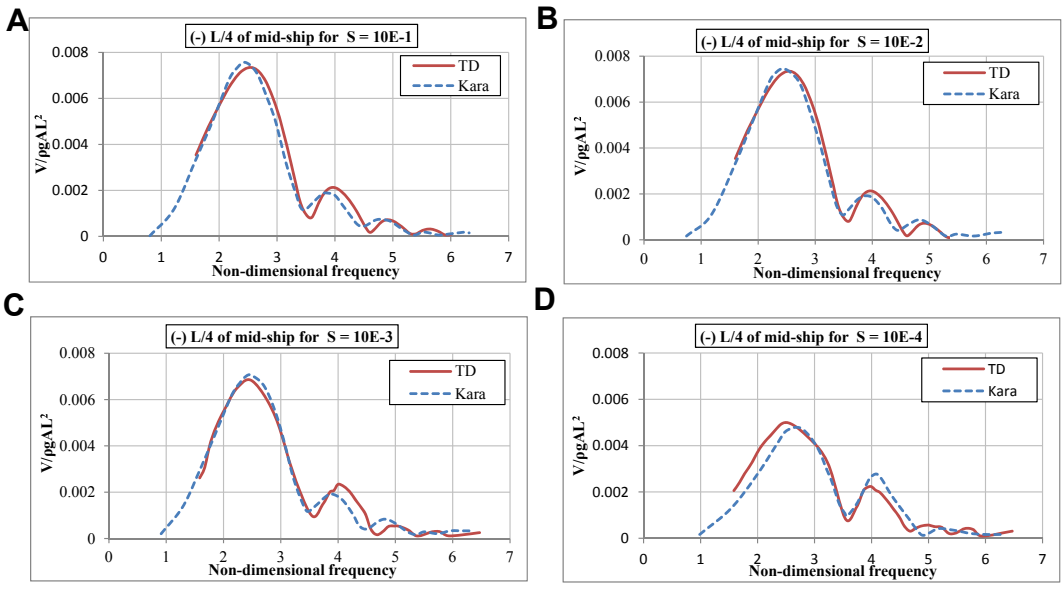

Fig. 12. (a)–(d). Vertical Shear Force transfer function at (−) L/4 of mid-ship of the Barge for stiffness factors.

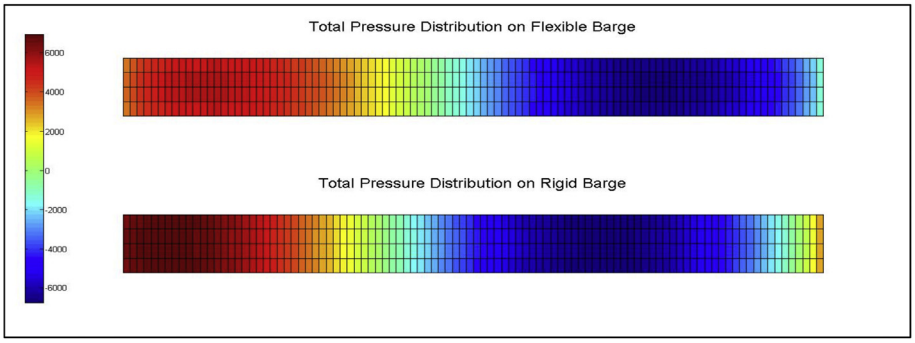

Fig. 13. Comparison of the pressure plots in case of flexible and rigid Barge at $\omega\sqrt{L/g}$= **2.5**.

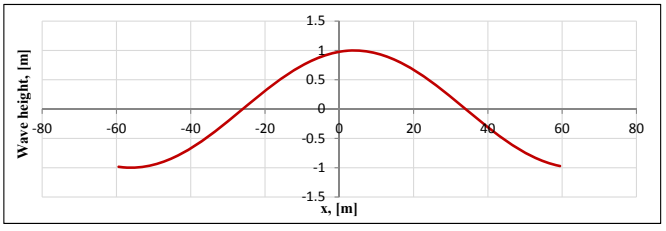

Fig. 14. Wave profile along the length of flexible and rigid barge at $\omega\sqrt{L/g}$= **2.5**.

Table 3
The principal characteristics of the Barge.

Item	Symbol	Value
Length over all (m)	*LOA*	150.0
Length between perpendiculars (m)	*LBP*	150.0
Breadth (m)	*B*	24.0
Depth (m)	*D*	15.0
Draught (m)	*T*	6.0
Displacement (tonnes)	*M*	22140.0
KG (m)		7.5
LCG from mid-ship (m)		0.0

hydrostatic force is extremely important.

To check the efficiency and the robustness of the present hydro-

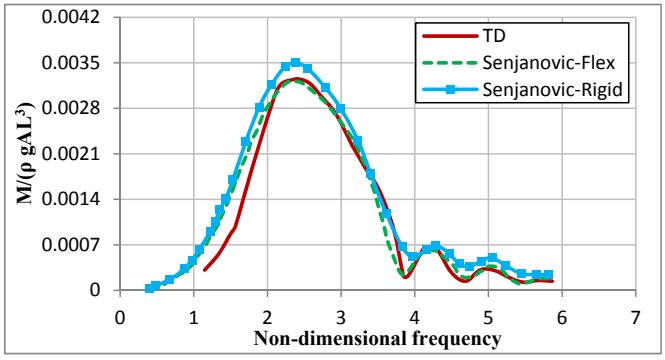

Fig. 15. Vertical Bending Moment transfer function for rigid and elastic Barge at mid-ship, $\beta = 150^{\circ}$.

elasticity code, displacements of the barge at forward perpendicular (FP), mid-ship, and aft perpendicular (AP) is computed and presented in Fig. 7 for $\omega\sqrt{L/g} = 2.5$. The stability of the results indicates the efficiency and robustness of the present formulation.

From Table 1, it may be noted that uniform mass distribution is taken for the Model I which can be considered as the simplest situation. The similar model and mass distribution are taken by Farstad (1997) and Kara (2015). However, Kara (2015) presented the results for different stiffness factors. Therefore, to start with, initial validation is done with the results

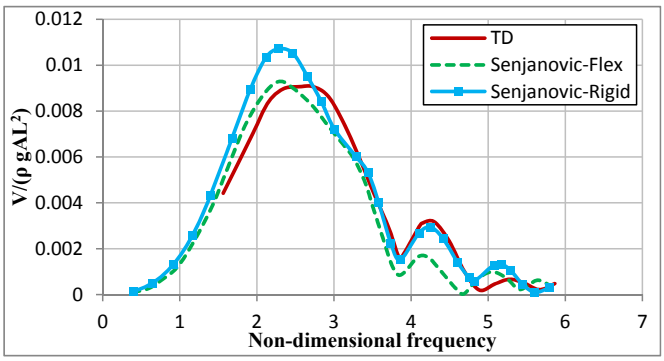

Fig. 16. Vertical Shear Force transfer function for rigid and elastic Barge at (+)L/4 of mid-ship, $\boldsymbol{\beta} = \mathbf{150}^{\circ}$.

Table 4
The main characteristics of the prismatic barge.

Item	Symbol	Value
Barge length (m)	*L*	2.445
Draught (m)	*T*	0.12
Total mass (pontoons + equipment) (kg)	*M*	171.77
Distributed mass (kg/m)	*m*	70.253
Bending stiffness of rod (N-m^2)	*EI*	175.0
Young's modulus of rod (N/m^2)	*E*	2.1E11

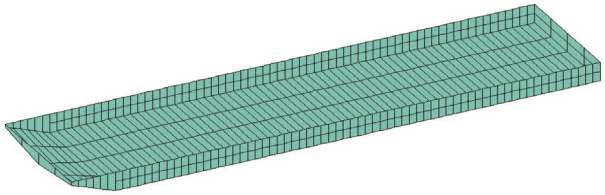

Fig. 17. Panel model of the segmented Barge.

Table 5
Dry natural frequencies (rad/sec) of the first four flexible vertical modes of the Barge.

Mode No.	TD	Senjanović et al. (2008a)
7	5.21	5.21
8	12.36	12.37
9	22.16	21.08
10	31.56	30.67

reported in Farstad (1997). Then shear forces at a particular section are computed for different stiffness factors and compared with that of Kara (2015). Fig. 8 shows the comparison of displacement RAOs (Response Amplitude Operators) at mid-ship. Farstad (1997) computed the

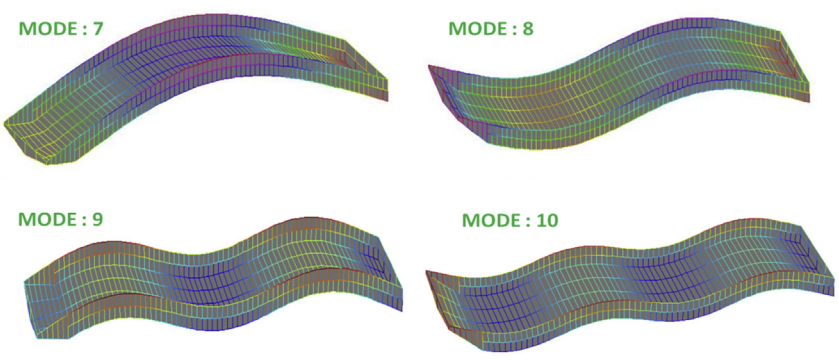

Fig. 18. Dry natural modes of flexible vertical vibration.

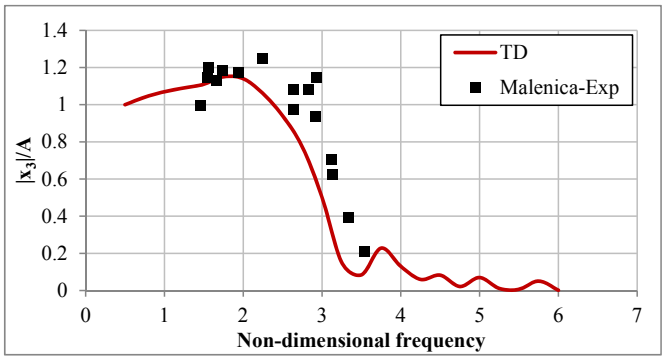

Fig. 19. Barge vertical displacement RAOs at bow with $\mathbf{F_n} = \mathbf{0.0}$ at head seas.

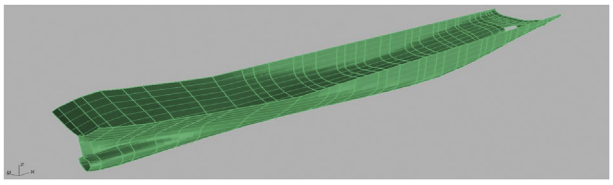

Fig. 20. Panel model of containership used for hydrodynamic analysis.

displacement, shear force, bending moment considering the first eight flexible modes. From the figure, it can be observed that both results agreed very well. Although some small difference may be noticed at higher frequency range, overall agreement is reasonably good. The vertical bending moment transfer function at mid-ship of the barge is plotted in Fig. 9. The result shows good assent with compared result. Similarly, the shear force transfer function for the barge at $x = -L/4$ and $x = +L/4$ are computed and presented in Fig. 10 and Fig. 11. The comparison shows quite good agreement with Farstad (1997). Apart from some slight variation in some frequency range, the overall agreement is excellent. Fig. 12a–d shows the vertical shear force at $x = -L/4$ with varying stiffness factor and compared with the results of Kara (2015). The stiffness factor S_f in this paper is defined as $EI/\rho g L^5$. From these figures also, it can be noted that overall agreement is extremely good with Kara (2015) results.

To check the influence of the flexibility in the hydrodynamic pressure, dynamic pressure plot is given in case of rigid and flexible body in Fig. 13 at $\omega\sqrt{L/g} = 2.5$. The schematic representation of the corresponding wave profile is given in Fig. 14. From Fig. 13, it is clearly seen that due to flexibility, the dynamic pressure changes significantly. This difference comes due to the change of the body boundary condition (14).

3.1.2. *Analysis of barge model II*

The second set of results is computed for a rectangular barge, where, the distribution of the mass is non-uniform. The geometric details and

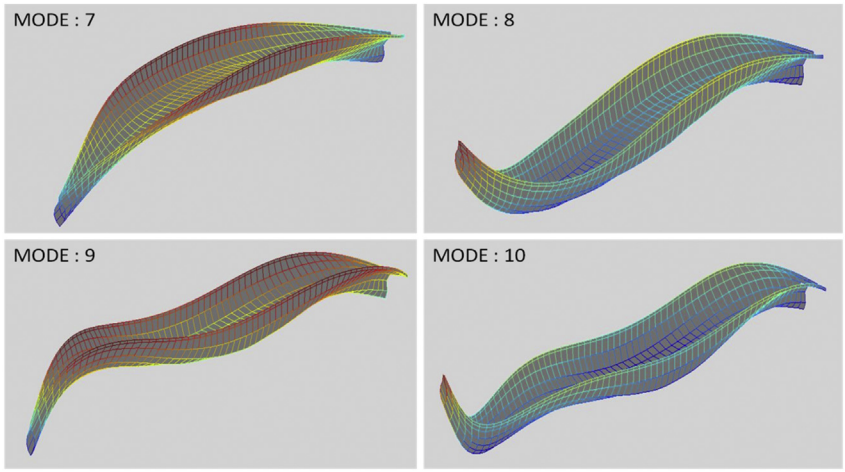

Fig. 21. Flexural modes of undamped vertical vibration.

Table 6
The main characteristics of the container ship.

Item	Symbol	Value
Overall Length (m)	*LOA*	300.9
Length between perpendiculars (m)	*LPP*	286.6
Breadth (m)	*B*	40
Depth (m)	*D*	24.2
Draught (m)	*T*	11.98
Displacement (tonnes)	*M*	85562.7
LCG from midship (m)		4.9
Radius of Gyration about x-axis (m)	k_{xx}	14.4
Radius of Gyration about y-axis (m)	k_{yy}	70.144
Radius of Gyration about z-axis (m)	k_{zz}	11.412

Table 7
Natural frequencies for vertical vibration of container ship (Hz).

Mode No.	$N_n = 50$	$N_n = 65$	$N_n = 100$
7	0.63	0.64	0.64
8	1.39	1.39	1.39
9	2.33	2.34	2.34
10	3.39	3.39	3.41

mass distribution are taken from the work reported by Senjanovic et al. (2013). The principal characteristics of this barge are given in Table 3. More detailed information about the structural arrangements is available in Senjanovic et al. (2013). In this case, the vertical bending moment at mid-ship and shear force at $(-L/4)$ of mid-ship is computed. The transfer functions for VBM and SF is plotted in Figs. 15 and 16 for the heading angle $\beta = 150^{\circ}$ and compared with reported numerical results. In the figures, "Senjanovic-Flex" and "Senjanovic-Rigid" refer the hydroelastic and rigid body results given by Senjanović et al. (2013). From the comparisons, it can be noted that, both the results agree excellently. Furthermore, it is interesting to note that bending moment results for the rigid body case are showing the higher peak. This trend indicates, assuming the structure to be rigid could lead to overestimating the bending moment and shear force results. However, this may not be true when the ship is considerably large and vertical, horizontal, and torsional modes are considered altogether.

3.1.3. Comparison with experiment for a segmented barge (model III)

Finally, the structural deflection of the barge is validated with the experimental results reported by Malenica et al. (2003). The principal dimension of the barge is given in Table 4. The details of the experimental model can be found out from Malenica et al. (2003). The hydrodynamic panel model for this barge is shown in Fig. 17. The experimental model consisting of 12 pontoons and were connected

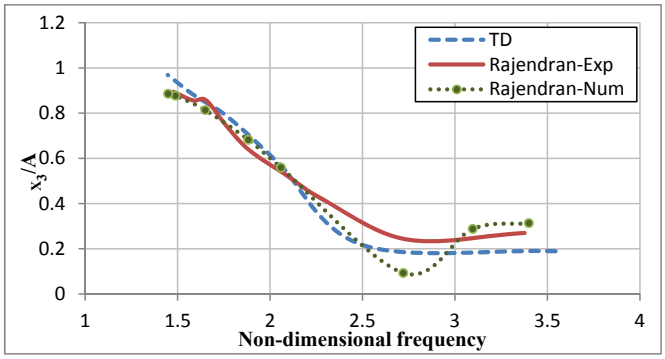

Fig. 22. Comparison of numerical and experimental vertical displacement RAOs.

together with a steel rod. However, for predicting the hydroelastic response, the gaps between the segmented pontoons are not considered.

In this case, also, the number of panels for hydrodynamic analysis and number of elements for finite element discretization has been considered by checking the convergence test. For instance, in Table 5 dry natural frequencies for vertical vibration of the model are compared with that of Senjanović et al. (2008a) and found satisfactory agreement between both the results. In Fig. 18, the dry natural modes of vertical vibrations are presented for the first four natural frequencies. Fig. 19 shows a comparison between the experimental and the computed results for displacement RAO at the bow of the barge at a heading angle $\beta = 180^{\circ}$. The comparison shows overall good agreement. However, there are some differences in mid frequency range, it may be due to the difference in

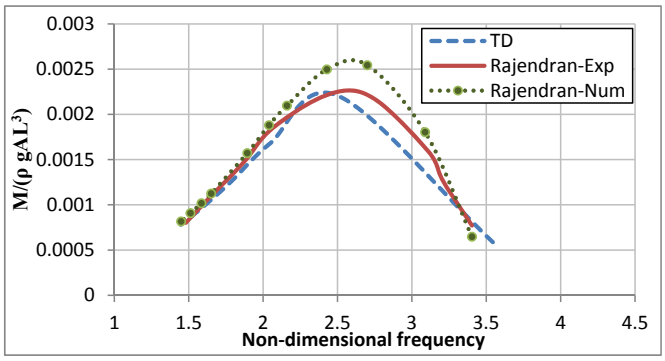

Fig. 23. Comparison of numerical and experimental vertical bending moment RAOs.

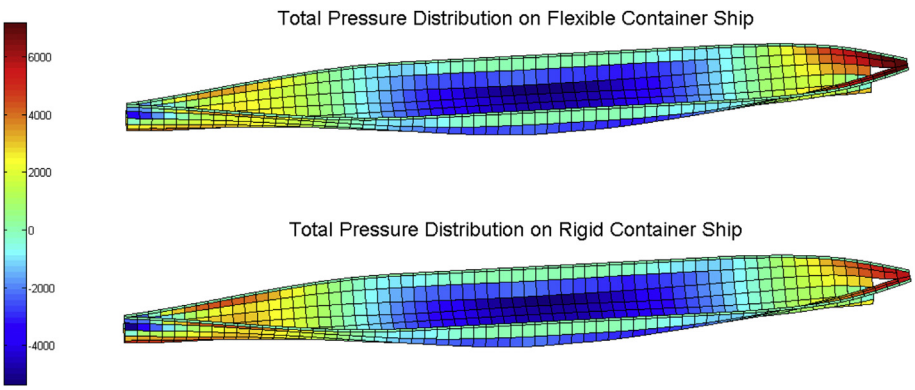

Fig. 24. Comparison of the pressure plot considering the container ship as flexible and rigid body for $\omega\sqrt{L/g}= 2.5$ (Distribution of pressure along panels is taken by considering the maximum pressure at mid-ship section panels).

numerical modelling with the experimental one, as the gaps between the segmented pontoons are not considered in the numerical model. Therefore, because of that modification, structural responses differ slightly from those of the experimental responses. However, from the overall pattern, it can be confirmed that the present numerical scheme captures the response reasonably good with engineering accuracy.

Therefore, from the barge results (Figs. 7–19), it can be concluded that the proposed methodology is capable of producing good results in case of simplistic hull shapes like a barge. However, it is required to validate the proposed method in case of realistic hulls also, which has been done in the following sections.

3.2. Comparison between numerical and experimental flexible responses of containership

The efficiency and robustness of the proposed work are verified for a large container ship (see Fig. 20). The vertical displacement, bending moment at mid-ship is computed and compared with published experimental and numerical results.

The geometric model of the hull, distribution of mass along the hull, and experimental results are taken from Rajendran and Guedes Soares (2016). The experimental model was divided into 8 segments, and each segment was connected together with an aluminum backbone of variable structural characteristics along the hull. However, like barge Model III, in this case, also, such connectivity is ignored. Fig. 21 shows the three-dimensional panel model of the containership. The main particulars of the ship are given in Table 6.

The dry natural frequencies are calculated numerically for the containership for convergence. Table 7 shows first four dry natural frequencies of the undamped free vibration of the hull and corresponding dry modes are shown in Fig. 21. The vertical bending moment and the displacement at mid-ship are computed and compared with the experimental and numerical results given by Rajendran and Guedes Soares (2016). In the plots 22 and 23, “Rajendran-Exp” and “Rajendran-Num” denote the experimental and numerical results given by Rajendran and Guedes Soares (2016).

In Fig. 22 displacements RAO at mid-ship is plotted. The overall good agreement is observed among all the results. Fig. 23 shows vertical bending moment RAO at mid-ship section. The figure shows the bending moment results computed by the present method agree excellently with the experiment. Therefore, from Figs. 22 and 23, it can be concluded that the present method is capable of getting accurate results for the realistic ship hull as well. Fig. 24 represents the dynamic pressure plot in case of the rigid and flexible body at the non-dimensional frequency $\omega\sqrt{L/g}= 2.5$, the corresponding wave profile is as same as Fig. 14. Though the difference is not very prominent in this case, still some difference can be seen between the rigid and flexible case which indicates the effect of structural flexibilities into the hydrodynamic solution.

4. Conclusion and future scope

In this paper, a direct BEM-FEM coupled method in time domain is developed for hydroelasticity analysis of floating bodies. A 3D time domain panel method is used to solve the hydrodynamic problem. Structural deflection is computed in time domain using FEM. Both the methods then coupled through body boundary condition in hydrodynamic solution. A simple but effective algorithm is developed to exchange the variables between structural and hydrodynamic code. To check the accuracy and implementation of the proposed scheme; three different barge type structures, and a large container ship are taken for the analysis. Structural deflection, shear force and bending moment are calculated and compared with available published and experimental results. It is seen that the present methodology compared very well with the published results. Also, it may be noted that the present scheme is able to produce very steady time domain results which confirm the efficiency and robustness of the present methodology. Therefore, one can conclude that the proposed coupled BEM-FEM scheme is efficient, robust and produce reasonably good results with engineering accuracy and could be a useful tool to assess the hydroelasticity effect on the structure while designing a vessel. Also from the results, it is observed that structural flexibility affect the hydrodynamic pressure on the hull. Therefore, the effect due to flexible nature of the structure must be considered when dynamic pressure load is estimated at design stage.

As a future scope, the present methodology can be further extended to include torsional and horizontal bending, certain non-linearities such as Frude-Krylov, nonlinear hydrostatic into the hydroelasticity solution.

Acknowledgements

This work was supported by Naval Research Board, India under Project No. NRB-344/HYD/14-15. Any opinions, findings and conclusions or recommendations expressed in this manuscript are those of the writers and do not necessarily reflect those of the Naval Research Board, India.

References

Andrianov, A.O.I., 2005. Hydroelastic Analysis of Very Large Floating Structures. Doctoral dissertation. Delft University of Technology, TU Delft.
Bishop, R.E.D., Price, W.G., 1979. Hydroelasticity of Ships. Cambridge University Press.
Cummins, W.E., 1962. The impulse response function and ship motions. Shiffstechnik 9, 101–109.
Datta, R., Sen, D., 2007. The simulation of ship motions using a B-Spline based panel method in time domain. J. Ship Res. 51 (3), 267–284.
Datta, R., Rodrigues, J.M., Soares, C.G., 2011. Study of the motions of fishing vessels by a time domain panel method. Ocean. Eng. 38 (5), 782–792.
Datta, R., Fonseca, N., Soares, C.G., 2013. Analysis of the forward speed effects on the radiation forces on a Fast Ferry. Ocean. Eng. 60, 136–148.
Farstad, T.H., 1997. Transient Seakeeping Analysis Using Generalized Modes. M.Sc. thesis. MIT.
Hirdaris, S.E., Price, W.G., Temarel, P., 2003. Two-and three-dimensional hydroelastic modelling of a bulker in regular waves. Mar. Struct. 16 (8), 627–658.

Iijima, K., Yao, T., Moan, T., 2008. Structural response of a ship in severe seas considering global hydroelastic vibrations. Mar. Struct. 21 (4), 420–445.
Karmakar, D., Bhattacharjee, J., Sahoo, T., 2009. Wave interaction with multiple articulated floating elastic plates. J. Fluid Struct. 25 (6), 1065–1078.
Kara, F., 2015. Time domain prediction of hydroelasticity of floating bodies. Appl. Ocean Res. 51, 1–3.
Kim, Y., Kim, K.H., Kim, Y., 2009. Analysis of hydroelasticity of floating shiplike structure in time domain using a fully coupled hybrid BEM-FEM. J. Ship Res. 53 (1), 31–47.
Kim, K.H., Bang, J.S., Kim, J.H., Kim, Y., Kim, S.J., Kim, Y., 2013. Fully coupled BEM-FEM analysis for ship hydroelasticity in waves. Mar. Struct. 33, 71–99.
Lin, W.M., Yue, D.K.P., 1990. Numerical solutions for large- amplitude ship motions in time domain. In: Proc. of the 18th Symposium on Naval Hydrodynamics (Ann Arbor, MI, USA).
Liu, M., Gorman, D.G., 1995. Formulation of Rayleigh damping and its extensions. Comput. Struct. 57 (2), 277–285.
Liu, S.W., Bai, R., Chan, S.L., 2016. Dynamic time-history elastic analysis of steel frames using one element per member. Structures 8, 300–309.
Malenica, S., Molin, B., Remy, F., Senjanović, I., 2003. Hydroelastic response of a barge to impulsive and non-impulsive wave load. In: Hydroelasticity in Marine Technology. Oxford, UK, pp. 107–115.
Meylan, M.H., Sturova, I.V., 2009. Time-dependent motion of a two-dimensional floating elastic plate. J. Fluid Struct. 25, 445–460.
Meylan, M.H., Tomic, M., 2012. Complex resonances and the approximation of wave forcing for floating elastic bodies. Appl. Ocean Res. 36, 51–59.
Newman, J.N., 1986. Distribution of sources and normal dipoles over a quadrilateral panel. J. Eng. Math. 20, 113–126.
Newmark, N.M., 1959. A method of computation for structural dynamics. J. Eng. Mech. Div. 85 (3), 67–94.
Rajendran, S., Guedes Soares, C., 2016. Numerical investigation of the vertical response of a containership in large amplitude waves. Ocean. Eng. 123, 440–451.
Sahoo, T., Yip, T.L., Chwang, A.T., 2001. Scattering of surface waves by a semi-infinite floating elastic plate. Phys. Fluids 13 (10), 3215–3222.
Sen, D., 2002. Time-domain computation of large amplitude 3D ship motions with forward speed. Ocean. Eng. 29 (8), 973–1002.
Senjanović, I., Malenica, Š., Tomas, S., 2008a. Investigation of ship hydroelasticity. Ocean. Eng. 35 (5), 523–535.
Senjanović, I., Tomić, M., Tomašević, S., 2008b. An explicit formulation for restoring stiffness and its performance in ship hydroelasticity. Ocean. Eng. 35 (13), 1322–1338.
Senjanović, I., Malenica, Š., Tomašević, S., 2009. Hydroelasticity of large container ships. Mar. Struct. 22 (2), 287–314.
Senjanović, I., Hadžić, N., Bigot, F., 2013. Finite element formulation of different restoring stiffness issues in the ship hydroelastic analysis and their influence on response. Ocean. Eng. 59, 198–213.
Seng, S., Jensen, J.J., Malenica, S., 2014. Global hydroelastic model for springing and whipping based on a free-surface CFD code (openFOAM). Int. J. Nav. Archit. Ocean Eng. 6, 1024–1040.
Sengupta, D., Datta, R., Sen, D., 2016. A simplified approach for computation of nonlinear ship loads and motions using a 3D time-domain panel method. Ocean. Eng. 117, 99–113.
Sengupta, D., Pal, S.K., Datta, R., 2017. Hydroelasticity of a 3D floating body using a semi analytic approach in time domain. J. Fluid Struct. 71, 96–115.
Squire, V.A., 2008. Synergies between vlfs hydroelasticity and sea ice research. Int. J. Offshore Polar Eng. 18 (4), 1–13.
Taghipour, R., Perez, T., Moan, T., 2009. Time-domain hydroelastic analysis of a flexible marine structure using state-space models. J. Offshore Mech. Arct. Eng. Trans. Asme 131 (1).
Wang, S., Karmakar, D., Soares, C.G., 2016. Hydroelastic impact of a horizontal floating plate with forward speed. J. Fluid Struct. 60, 97–113.
Wu, M., Moan, T., 1996. Linear and nonlinear hydroelastic analysis of high-speed vessels. J. Ship Res. 40 (2), 149–163.